THE ASTROPHYSICAL JOURNAL, 410:188–201, 1993 June 10

THE FORMATION OF CYANOPOLYYNE MOLECULES IN IRC +10216

ISABELLE CHERCHNEFF,[1] ALFRED E. GLASSGOLD,[1] AND GARY A. MAMON[2]
Received 1992 September 28; accepted 1992 December 14

ABSTRACT

Molecule formation in the outer envelope of the carbon-rich star IRC +10216 is investigated, with special emphasis on the chemistry of the cyanopolyynes HC_iN ($i = 3, 5, 7$). Basic elements of the photochemical model of Glassgold, Lucas, & Omont are revised. A dust model suitable to IRC +10216 is used, for which the extinction properties in the far-UV are those of 500 Å amorphous carbon particles.

A new chemical route to the formation of large cyanopolyynes is proposed, based on reactions of the radicals C_3N and C_5N with acetylene, and shown to be efficient. Our results agree qualitatively with observations of the spatial distributions of HCN, CN, HC_3N, and C_3N, but the calculated column densities of the higher-order cyanopolyynes appear to be too small. The amount of the allenic radical HC_2N produced by molecular ion reactions with atomic N agrees with recent observations.

Subject headings: circumstellar matter — ISM: molecules — molecular processes — stars: carbon — stars: individual (IRC +10216)

1. INTRODUCTION

Owing to its proximity ($d = 150$–200 pc) and its large mass-loss rate, the evolved carbon-rich star IRC +10216 is one of the best-studied objects in the sky at infrared and radio wavelengths. Its circumstellar envelope is characterized by a rich and diverse chemistry that depends on position in the envelope: local thermodynamic equilibrium holds in the dense and warm layers just above the photosphere, grain-surface reactions characterize the intermediate region of the envelope, and the external interstellar radiation field initiates a rich photochemistry in the outer layers.

More than 40 chemical species have been detected so far in infrared absorption and millimeter emission, including complex rings and chains, and refractory compounds (see, e.g., the recent review by Lucas 1992). Chemical modeling of the IRC +10216 outer envelope has been carried out by Glassgold, Lucas, & Omont (1986, hereafter GLO), Nejad & Millar (1987), Glassgold et al. (1987, hereafter GMOL), and Howe & Millar (1990). An important result of these models is the shell distribution of chemical species synthesized as a result of molecular photodissociation and predicted earlier by Huggins & Glassgold (1982). Interferometric observations (see, e.g., Bieging & Rieu 1988; Lucas 1992) have confirmed this striking feature of molecular abundances at large distances. These and other supporting data suggest that the photochemical model is a promising way of interpreting observations of circumstellar molecules.

One challenging aspect of the chemistry of IRC +10216 is the origin of the many long-chain molecules. Among these are the cyanopolyynes (HC_iN, with $i = 3$–11), all of which have been detected. Various authors (e.g., Cernicharo et al. 1987) have interpreted the observations to provide evidence for a general decrease of the cyanopolyyne beam-averaged column densities with molecular size. However, none of the theoretical models mentioned previously have reproduced this abundance sequence.

The present paper investigates the cyanopolyyne chemistry in IRC +10216, in the context of a significantly improved photochemical model. Although the general ideas behind the model are similar to GLO (and the other studies referred to earlier), the execution of the model is made more realistic by a new approach to the calculation of photodissociation rates and by the use of dust extinction properties that are more appropriate for IRC +10216. We also consider the possible effects of changing the ambient UV radiation and the cosmic-ray ionization rate. In addition to the general update of the envelope chemistry in light of recent experimental or theoretical results, we also introduce a new chemical route for the formation of cyanopolyynes.

2. THE PHOTOCHEMICAL MODEL

The present study of the cyanopolyyne chemistry in the envelope of IRC +10216 is based on a photochemical model developed over the last decade. Although the importance of envelope shielding of the UV dissociating radiation was emphasized to start (e.g., Huggins & Glassgold 1982), a largely *phenomenological* approach was followed in practice. For example, the early discussion on the C_2H_2 and HCN photochains (Huggins, Glassgold, & Morris 1984; GLO; GMOL) described the envelope shielding for a chemical species i by a "shielding length" d_i and the corresponding photorate by

$$G_i(r) = G_i^0 \exp(-d_i/r), \quad (1)$$

where G_i^0 is the unshielded rate. These studies assumed that the radial variation of the all photorates was the same and even that the shielding lengths for the different species were identical. These symplifying assumptions were originally justifiable by the lack of information on the wavelength dependence of the underlying cross sections and the absence of extensive high spatial resolution maps of molecular emission lines in IRC +10216. However, this approach is no longer adequate because the shielding in the envelope depends strongly on wavelength. Furthermore, numerous projects to spectrally map IRC +10216 are now underway with large mm wave telescopes, using both single dishes and arrays (e.g., Lucas 1992; Bieging & Tafalla 1992).

Some improvements in the treatment of envelope shielding have already been made. For example, Morris & Jura (1983) took into account the nonradial transfer of the dissociating radiation and obtained an improved expression for dust shield-

[1] Department of Physics, New York University, 2 Washington Place, New York, NY 10003.
[2] DAEC, Observatoire de Meudon, F-92195 Meudon Cedex, France.

ing compared to equation (1). Even more important was the introduction of line self-shielding for carbon monoxide (Morris & Jura 1983; Mamon, Glassgold, & Huggins 1988). The present paper reconsiders the important roles of molecular photo cross sections and dust extinction for obtaining a quantitative description of continuum shielding.

2.1. *Astrophysical Parameters*

Table 1 lists the model parameters considered in this study, which are similar to previous usage. The distance $d = 200$ pc is almost standard but arbitrary. Zuckerman, Dick, & Claussen (1986) have argued for a smaller distance (~ 150 pc) in order for IRC +10216 not to be overluminous relative to most other carbon stars on the asymptotic giant branch. The expansion velocity and mass-loss rate are taken from the analysis of Huggins, Olofson, & Johansson (1988) and are accurate to 1 km s^{-1} and a few 10^{-5} $M_\odot$ yr^{-1}, respectively. We use the same temperature law as that of Mamon et al. (1988). Because the present model applies only beyond the region of dust formation, the abundances in Table 1 do not refer to the stellar photosphere but to the beginning of the outer envelope, $r = 1 \times 10^{15}$ cm (or ~ 10 R_*). The abundances of the well-bound molecules entering the outer envelope are regarded as phenomenological parameters, to be determined from observations. For the sake of consistency, we use only molecular abundances derived from mm line observations.

The CO abundance is reasonably well determined from analyses of extensive measurements of its emission in the $J = 1$–0 and 2–1 lines, which also measure the mass-loss rate; the value in Table 1 comes from Huggins et al. (1988). For HCN, we use the abundance deduced for the outer envelope by Bieging, Chapman, & Welch (1984) from interferometric measurements, after scaling to our mass-loss rate. Because C_2H_2 has no radiofrequency spectrum, we derive its abundance from that of the radical C_2H produced by C_2H_2 photodissociation. Bieging & Rieu (1988) determined a peak C_2H abundance of about 1.8×10^{-6} for a mass-loss rate of 4×10^{-5} $M_\odot$ yr^{-1}. After correcting to our mass-loss rate and multiplying by the *theoretical ratio* of initial acetylene to peak C_2H abundances, $(C_2H_2)_0/(C_2H)_p = 5/3$ (obtained by numerical modeling), we obtain $x(C_2H_2)_0 = 4 \times 10^{-6}$. Truong-Bach et al. (1987) carried out a similar analysis of their single-dish C_2H data, and their results, after renormalization to our model, correspond to $x(C_2H_2)_0 = 9 \times 10^{-6}$. We adopt an intermediate value in Table 1. Because of the limitations in the measurements and the interpretations, the HCN and C_2H_2 abundances are both uncertain by factors of at least 2–3.

Our previous choice of initial abundances relied to some degree on the results of near-IR absorption spectroscopy, a procedure that leads to uncertain results when the lines are highly saturated, which is the case for CO, C_2H_2, and HCN. Recent measurements by Keady & Ridgway (1991) and Wiedemann et al. (1991) give HCN and C_2H_2 abundances that are an order of magnitude larger than those listed in Table 1. On the assumption that the IR observations probe deep into the envelope, the difference may be ascribed to chemistry associated with dust grains, as well to the intrinsic uncertainties in the abundance determinations in the radio and the infrared.

TABLE 1

ENVELOPE PARAMETERS FOR IRC +10216

Distance	$d = 200$ pc
Expansion velocity	$V = 14$ km s^{-1}
Mass-loss rate (total hydrogen)	$\dot{M} = 3 \times 10^{-5}$ $M_\odot$ yr^{-1}
Gas density, $n = Cr^{-2}$	$C = 6.43 \times 10^{37}$ cm^{-1}
CO	3×10^{-4}
C_2H_2	6.7×10^{-6}
HCN	4×10^{-6}
N_2	1×10^{-4}

2.2. *Chemical Kinetics Calculation*

The chemical kinetics is described by a set of coupled, continuity equations of the generic form

$$v \frac{d}{dr} x(Y) = P(Y) - D(Y)x(Y) , \qquad (2)$$

where P and D are the production and destruction rates of species Y. These equations are solved by a general purpose circumstellar chemistry program (Glassgold, Mamon, & Huggins 1991) that also treats the associated radiative transfer. The version adopted here assumes steady, spherically symmetric outflow with constant hydrogen mass-loss rate $\dot{M}$. The flow velocity is set equal to the terminal velocity V so that the total number of hydrogen nuclei is given by $n(r) = C/r^2$, with $C = \dot{M}/4\pi m_H V$.

2.3. *Photo Cross Sections and Rates*

The photo processes included in the present chemical scheme are listed in Appendix A. The rates were calculated by integrating the mean radiation intensity $J_\lambda(r)$ at each point in the envelope over the associated wavelength dependent cross section (see the next section). Only a few of the required cross sections have been measured in the laboratory. Absorption cross sections have been measured for two important species, HCN and C_2H_2, and are labeled "E" in Appendix A. Theoretical calculations have been made for C_2H and C_2 and are labeled "T" in Appendix A. For other species, we have taken the latest theoretical estimates available in the literature or made "educated" guesses, referred to as "estimated" in Appendix A. Because of the lack of spectroscopic data on these species, we continue to assign these rates to the first wavelength band extending from 912 to 1100 Å (defined below in § 2.4), as done in GLO and GMOL.

The unshielded rates in Appendix A agree with those adopted for the interstellar medium, for example, by van Dishoeck (1988). However, they differ systematically from those used in earlier versions of the photochemical model by GLO and GMOL, typically by factors of a few. This difference, already mentioned by GLO, arises from the fact that most other studies, starting with Lee (1984), have assumed that the measured absorption and dissociation cross sections are the same, which results in large photorates. This seems to be borne out in the case of HCN, where the cross section for the production of excited CN approaches the total absorption cross section. Although this issue can only be settled by laboratory experiments for each molecule, we take dissociation equal to absorption ($\sigma_{diss} \cong \sigma_{abs}$), consistent with the consensus of previous workers. The most striking change occurs for acetylene, whose photodissociation rate is ~ 10 times larger than in GLO.

2.4. *Envelope Shielding*

We describe here a major improvement in the treatment of the envelope shielding. Earlier calculations used photorates characterized by the single exponential function of equation (1). In view of the unknown far-UV optical properties of cir-

cumstellar dust, the shielding lengths d_i were regarded as phenomenological parameters, and most of them were taken to be equal. In the present work the wavelength dependence of the photo cross sections is taken explicitly into account. We bin the relevant far-UV spectrum from 912 to 2500 Å into a set of bands labeled by the index k. Thus, the photorate G_j for process j is a sum over bands,

$$G_j(r) = \sum_k G_{j,k}^{(0)} \exp\left[-\tau_k(r)\right], \quad (3)$$

where $G_{j,k}^{(0)}$ is the unshielded rate and $\tau_k(r)$ is the total optical depth, measured from the outside, for the band k. The main contribution of $\tau_k(r)$ comes from dust, although atomic or molecular absorbers can contribute. Since the optical depth is a complex function of r, the photorate in equation (3) no longer has a simple exponential dependence. For example, the optical depth due to dust is a strong function of inverse wavelength $1/\lambda$ in the far-UV, and shorter wavelengths will be preferentially blocked by the envelope.

In line with this discussion, we note that GLO and other circumstellar chemistry models used a *one-band* approximation, with the band centered near 1000 Å, and, consequently, the envelope was overshielded. A similar criticism could be made of many interstellar chemistry models. The change from one to many bands can have a profound effect on the spatial distribution of chemical abundances of species that are destroyed at longer wavelengths. The details depend strongly on the optical properties of dust grains and on the spectrum of UV radiation incident on the circumstellar envelope.

2.5. *Dust Properties*

The physical and chemical properties of circumstellar dust are still poorly understood. In particular, there is no direct observational information on the far-UV dust extinction of IRC +10216. The observed spectral energy distribution from 0.5 to 1000 μm is well reproduced by amorphous carbon (AC) grains, rather than crystalline graphite particles (Sopka et al. 1985; Le Bertre 1987; Martin & Rodgers 1987). As discussed earlier, previous work with the photochemical model followed a phenomenological approach to dust shielding, guided in part by the observed far-UV properties of *interstellar* dust. However, circumstellar and interstellar dust are different. We consider AC grains to be the most important component of the dust in IRC +10216 and use recent theoretical and laboratory work to obtain the required far-UV optical properties.

Rouleau & Martin (1991) have developed a new modeling technique that includes shape and clustering effects and permits the calculation of the optical properties of AC dust grains for wavelength regions not covered by laboratory experiments, particularly below 1200 Å. These authors have kindly extended their calculations to small particles with radii, 10 Å $\leq a \leq$ 100 Å, and some of their results are shown in Figure 1. The extinction per unit volume from 1000 to 2000 Å is almost independent of size for small grains with $a \leq 100$ Å (not shown). Thus, details in the size distribution of the dust particles are unimportant as long as the grains are small ($a \leq 100$ Å). Figure 1 also shows the results of a recent laboratory experiment for AC particles with a size distribution peaking at 40 Å (Colangeli et al. 1992); there is a good correspondance with the calculations of Rouleau & Martin (1991) for small particles. However, the large UV extinction measured by Colangeli et al. may be due to scattering by small particles in their experiment. In § 4.2.2, we shall discuss the difference

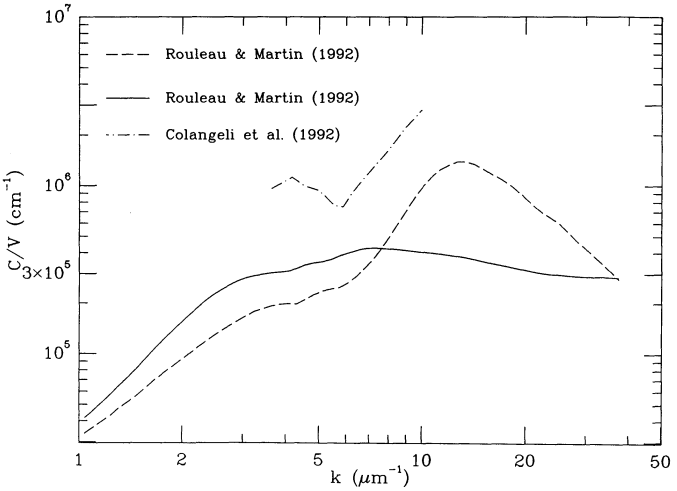

FIG. 1.—Dust extinction versus wavenumber for two models of Rouleau & Martin (1991) and the experiment of Colangeli et al. (1992), as discussed in the text. For the model of Rouleau & Martin, the particle sizes are $a = 100$ Å (*dashed curve*) and $a = 500$ Å (*solid curve*). The Colangeli experiment uses a distribution of particles with a mean size of 40 Å.

between small and large particles from the point of view of the effects on the spatial distribution of molecules predicted by the photochemical model.

The extinction cross section per unit volume in Figure 1 has been expressed in terms of the extinction efficiency $Q_e(\lambda, a)$,

$$\frac{C}{V} = \frac{3}{4}\frac{\langle Q_e(\lambda, a)a^2\rangle}{\langle a^3\rangle} \approx \frac{3}{4}\frac{Q(\lambda, a)}{a}. \quad (4)$$

Typical values for $Q(\lambda, a)/a$ at 1000 Å are $\sim 10^6$ cm^{-1} for "small" particles ($a \leq 100$ Å) and $\sim 4 \times 10^5$ cm^{-1} for "large" particles ($a \geq 500$ Å). We also need to specify the amount of dust present in the envelope, and we use the usual dust-to-gas mass ratio,

$$\frac{\rho_d}{\rho_g} = \frac{12[x_C - x_O - x_m(C)] + 32x_{Si}}{x_H + 4x_{He} + 28x_O + 12x_m(C)}, \quad (5)$$

where x_X is the total abundance of element X (X = H, He...), and x_m(C) is the abundance of carbon in gas phase molecules not in CO. Equation (5) is based on the simplifying assumption that, in IRC +10216, all of the oxygen is locked up in gas phase CO and all of the silicon is in dust. Adopting the parameters, $x_C \approx 7 \times 10^{-4}$, $x_O = 3 \times 10^{-4}$, $x_m(C) = 2 \times 10^{-5}$, and $x_{Si} = 4 \times 10^{-5}$, we obtain

$$\frac{\rho_d}{\rho_g} = 4.5 \times 10^{-3}, \quad (6)$$

about 20% larger than the estimate of Martin & Rodgers (1987), based on observations of the 11 μm continuum and the CO mm lines. It is possible to obtain a larger dust-to-gas ratio by increasing x_C, but any additional carbon dust must not emit as strongly in the infrared as the basic AC dust component.

The dust optical depth can be expressed as

$$\tau(\lambda) = \left(\frac{\rho_d}{\rho_g}\right)\frac{m_g}{\rho_{int}}\frac{C(\lambda)}{V}N_H, \quad (7)$$

where m_g is the mean mass of gaseous species per proton, ρ_{int} is the mean (internal) density of the dust particles, and N_H is the

hydrogen column density. For an optical depth of unity at 1000 Å, we have

$$N_{\rm H}^{(1)} = \left(\frac{\rho_d}{\rho_g}\frac{m_g}{\rho_{\rm int}}\frac{C}{V}\right)^{-1} . \quad (8)$$

Using the approximate values $m_g = 2.2 \times 10^{-24}$ g and $\rho_{\rm int} = 1.86$ g cm^{-3}, we find that $N_{\rm H}^{(1)} = 1.9 \times 10^{20}$ cm^{-2} for $C/V = 10^6$ cm^{-1} (small dust particles) and $N_{\rm H}^{(1)} = 4.7 \times 10^{20}$ cm^{-2} for $C/V = 4 \times 10^5$ cm^{-2} (large dust particles). The corresponding column density for previous models (e.g., GLO) is $\sim 4 \times 10^{20}$ cm^{-2}; the small grains produce more extinction at 1000 Å. However, as discussed above, the difference in wavelength dependence between small and large grains is also important.

2.6. *The Local Radiation Field*

Little is known about the local radiation field responsible for photo processes in the outer envelope of IRC +10216. Previous studies assumed that it is the same as the mean interstellar radiation field at the Sun. On exception is the analysis by Martin & Rodgers (1987) of the radial variation in the intensity of a CCD image due to Crabtree, McLaren, & Christian (1987). Using their AC dust model, Martin & Rodgers concluded that the radiation field in the neighborhood of IRC +10216 was about 5 times weaker than at the Sun.

The properties of the UV radiation in the solar vicinity have been reviewed recently by Gondhalekar (1990), who showed that the field is strongly anisotropic and inhomogeneous. The mean field is usually described by the expression derived by Draine (1978). The local field at IRC +10216 (Galactic coordinates $l = 221°$, $b = 45°$) should be the same order of magnitude as the field at the Sun because the stellar sources are the same, bright, blue Orion stars. This conclusion is confirmed by examining the statistical data given by Gondhalekar (1990) and by searching the bright star catalogs for additional sources. There are four late-type B stars within 60 pc of IRC +10216 but they make a negligible contribution to the radiation field.

Turning to the distribution of molecular clouds, CO sky surveys of the region of interest for the present work ($l = 190°$–$250°$) show no evidence for high molecular gas concentrations at positive Galactic latitudes and at distances close to IRC +10216 (May, Murphy, & Thaddeus 1988). This is supported by the survey of high-latitude molecular clouds carried out by Magnani, Blitz, & Mundy (1985). However, Désert, Bazell, & Boulanger (1988) have identified infrared-excess clouds at high latitudes in the directions of IRC +10216, so that it is premature to rule out the presence of dust along the line of sight from the Orion OB association to the star.

Most of the calculations in this paper are based on the Draine radiation field, but we consider two variations from this standard field. The first one involves an increase by an overall factor of 3 and is motivated by the fact that IRC +10216 is closer to the Orion stars than the Sun. The second variation is suggested by the analysis by Martin & Rodgers (1987) and by the possible presence of molecular gas along the line of sight from the Orion stars to IRC +10216. These variations will be discussed in § 4.2.1.

3. CHEMISTRY

The chemical properties of the envelope of IRC +10216 are determined by three types of processes: (1) chemical reactions with high activation energy in the dense upper photosphere and the inner envelope ($r \sim 1$–$3R_*$); (2) dust grain-surface and gaseous radical chemistry in the intermediate layers ($r \sim 3$–$10R_*$); and (3) photochemistry in the outer envelope ($r > 10R_*$). As discussed in § 2, the effects of the first two regions are expressed by phenomenological initial abundances for the gas flowing into the outer envelope. Earlier papers on the photochemical model show that the species at large stellar radii can be classified as "progenitors" or "products." The progenitors are exemplified by stable molecules such as CO, C_2H_2, and HCN, which have abundance distributions in space that are sharply cutoff due to photodissociation. Product species, formed by photodissociation and subsequent chemical reactions, for example, C_2H and CN, have peaked or shell distributions. An important issue for the theory is to determine the progenitor species. Table 1 presents a minimal set of species directly involved in the cyanopolyyne chemistry. Keady & Ridgway (1991) have recently presented evidence from infrared spectroscopy that extends this list to include CS and SiO, formed in the upper atmosphere of the star, and NH_3, CH_4, and SiH_4, produced in the inner envelope.

Another basic question for the chemistry of the outer envelope is the relative importance of ion-molecule and radical-molecule reactions (Lafont, Lucas, & Omont 1982). Fast ion-molecule reactions, familiar in the interstellar medium, were emphasized at first. However, improved laboratory data on radical-molecule reactions have shown that the somewhat lower rate coefficients of these reactions are easily made up by the much larger abundances of neutral radicals compared to molecular ions, thereby leading to larger net reaction rates. The presence of cyanopolyynes in carbon-rich circumstellar envelopes has not yet been satisfactorily explained. Both theoretical and observational studies on IRC +10216 provide an excellent opportunity for understanding their chemistry because several members of their family, notably HC_3N, C_3N, and HC_5N, can be measured in detail with large telescopes and interferometers at mm wavelengths. Discussions of the interesting aspects of hydrocarbon chain and silicon chemistries are postponed for later papers (see, however, the preliminary report by Glassgold & Mamon 1992).

The ion-molecule chemistry of the simpler cyanopolyynes was first discussed by GLO and Nejad & Millar (1987). Cyanoacetylene (HC_3N) production was initiated by the reaction of HCN and CN with acetylenic ions ($C_2H_2^+$ and $C_2H_3^+$). Nejad & Millar concluded that this mechanism and other ionic pathways produce little HC_3N because of the small molecular ion abundances present in the envelope. Howe & Millar (1990) were able to reproduce the observed beam-averaged column density of HC_3N in the outer envelope with the radical-molecule reaction[3]

$$CN + C_2H_2 \rightarrow HC_3N + H , \quad (R199)$$

whose rate coefficient has been measured by Lichtin & Lin (1986). Howe & Millar (1990) also proposed that cyanodiacetylene (HC_5N) and cyanotriacetylene (HC_7N) are formed by the generalization of Reaction 199 to C_4H_2 and C_6H_2,

$$CN + C_4H_2 \rightarrow HC_5N + H , \quad (R200)$$

and

$$CN + C_6H_2 \rightarrow HC_7N + H , \quad (R201)$$

neither of which has been measured in the laboratory.

[3] All the reactions referred to in the text are numbered following Appendix B.

In the present work, we propose a new neutral production route for the formation of the large cyanopolyynes (HC_5N and HC_7N), which is based on a different kind of generalization of Reaction 199 in which C_iN radicals ($i = 3, 5\ldots$) replace CN. Thus, HC_5N is formed by

$$C_3N + C_2H_2 \rightarrow HC_5N + H\,, \qquad \text{(R204)}$$

and HC_7N is formed by

$$C_5N + C_2H_2 \rightarrow HC_7N + H\,. \qquad \text{(R205)}$$

The exothermicity of these reactions has been checked against new thermodynamic data compiled by Cherchneff & Barker (1992). Reactions 204 and 205 had been previously ruled out by Lafont et al. (1982) on the basis of old thermodynamic data. The rate coefficients for these reactions have not yet been measured in the laboratory, but acetylene attachment on C_3N and C_5N radicals should occur in a similar way to CN. In the absence of other information, we have chosen the rate coefficients for Reactions 204 and 205 to be about the same as for Reaction 199 (see Appendix B).

Although Bieging & Rieu (1988) presented evidence for a shell distribution for HC_3N, they found that its abundance was not negligible in the inner envelope. One possibility is that HC_3N is formed in the upper atmosphere of the star and survives passage to the outer envelope. The thermal equilibrium calculations of Cherchneff & Barker (1992) suggest inner envelope ("injected") abundances for HC_3N of the order of 10^{-9} to 10^{-8}. The abundance of HC_3N interior to the peak is also influenced by the dissociative recombination of H_2CN^+, an ion produced by proton transfer from the cosmic-ray ion H_3^+ to HCN (GMOL),

$$H_2CN^+ + e^- \rightarrow CN + H_2\,. \qquad \text{(R56)}$$

The branching of this reaction to CN affects HC_3N production by Reaction 199 at small radii, where the H_2NC^+ abundance is large due to the small electron concentration in this region.

The HC_2N radical has been recently detected in IRC +10216 (Guélin & Cernicharo 1991). Because of its allenic structure (the bond between the two C-atoms is double), HC_2N does not belong to the cyanopolyyne family. It is of interest, however, to consider its synthesis as well as that of the related radicals H_2C_2N and C_2N, and of higher order chains of the form $H_mC_{2n}N$. The laboratory experiments of Federer et al. (1986) suggest the following set of reactions for H_2C_2N and HC_2N formation [already proposed by Irvine et al. (1988) to explain the presence of H_2C_2N in molecular clouds]

$$C_2H_4^+ + N \rightarrow H_3C_2N^+ + H\,, \qquad \text{(R186)}$$

followed by

$$H_3C_2N^+ + e^- \rightarrow H_2C_2N + H\,, \qquad \text{(R61)}$$

or

$$H_3C_2N^+ + e^- \rightarrow HC_2N + H + H\,. \qquad \text{(R62)}$$

The formation of HC_2N depends on the branching ratios of Reactions 61 and 62. The radical C_2N can be produced by a similar set of reactions involving $C_2H_2^+$ and N.

In addition to the new chemical pathways discussed in this section, we have extended the chemical reaction network and updated the rate coefficients. The chemical reactions are documented in Appendix B.

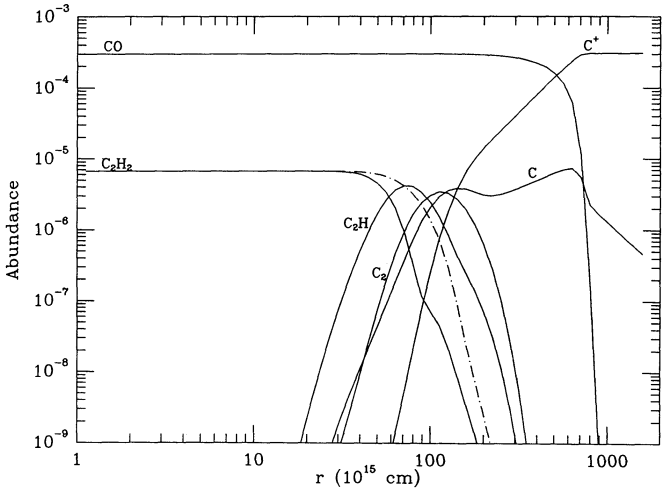

FIG. 2.—The abundances for the CO and C_2H_2 photochains for the standard model. The dot-dashed curve is the C_2H_2 abundance for the C_2H_2 photodissociation rate used in GLO.

4. RESULTS

4.1. *The Standard Case*

We introduce a standard case for the circumstellar envelope of IRC +10216 in order to study how various physical quantities affect the abundances calculated with the photochemical model. It is defined by the parameters in Table 1 and by the following choices: (1) the average interstellar radiation field is the Draine (1978) field, as discussed in § 2.6; (2) the dust extinction properties in the far-UV are those of 500 Å AC grains, as computed by Rouleau & Martin (1991) and discussed in § 2.5; and (3) the cosmic-ray ionization rate per H_2 molecule is $\zeta = 5 \times 10^{-18}$ s^{-1}. The results for the major species of the acetylene and the cyanopolyyne chemical families are presented in Figures 2 and 3. To underscore the importance of our new radiation transfer procedures, the dot-dashed curve in Figure 2 shows the effects of using a one-band model for the

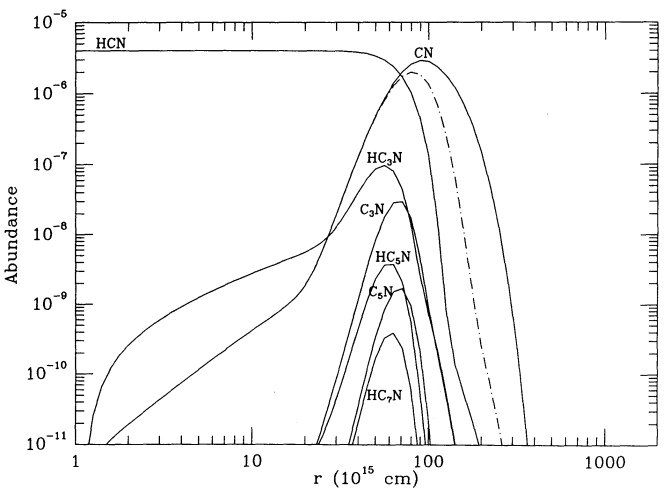

FIG. 3.—The abundances for the HCN photochain for the standard model. The dot-dashed curve is the CN abundance for the CN photodissociation rate of Lavendy et al. (1987).

photodissociation of C_2H_2 with the rate used in earlier work, that is, $G_{diss}(C_2H_2) = 4 \times 10^{-10}$ s^{-1}, about 8 times smaller than the value listed in Appendix A.

The results in Figures 2 and 3 curves are generally similar to previous calculations but there are some quantitative differences. The main one is that the photochemical region has been shifted outwards due to the improvements in the theory of envelope shielding and dust extinction discussed in § 2. For example, the peak positions of the second generation species, C_2H and CN, occur at $r = 7.5 \times 10^{16}$ and 9.5×10^{16} cm, respectively, which corresponds to angular distances of 25″ and 30″ (for $d = 200$ pc). The results correspond in a rough way to the present observational situation for these two radicals. For example, Bieging & Rieu (1988) deduced a broad shell distribution for C_2H with a peak at ~20″, and Truong-Bach et al. (1987) deduced from crude maps that the CN distribution was much larger than that for C_2H. We can of course not make any detailed comparison between the peak C_2H abundances deduced by the observers because we have adjusted the initial C_2H_2 abundance to agree with their values. On the other hand, the theory does account roughly for the peak CN abundance; in this case, the initial HCN abundance was deduced from the observations of Bieging et al. (1984). Basically, the photochemical model for IRC +10216 predicts that the peak CN abundance is close to the initial HCN abundance.

It would be premature to seek very close agreement between theory and observation at this point because of the numerous uncertainties in both the observations and the theory. To obtain true abundance distributions from observations requires spectral mapping in at least two lines so that both the excitation temperature and the abundance can be determined. On the other hand, the utility of the theory is restricted by our lack of knowledge of photodissociation rates for radicals and other exotic molecules and of the far-UV properties of circumstellar dust. In this connection, we have adopted the photo cross section estimate of van Dishoeck (1988) for CN, which gives the relatively small rate in Appendix A, $G_0(CN) = 2 \times 10^{-10}$ s^{-1}. The theory of CN photodissociation by Lavendy, Robbe, & Gandara (1987) yields a higher rate, 7×10^{-10} s^{-1}. The CN distribution for this larger rate is given as the dot-dashed curve in Figure 3. A line excitation calculation would be needed to assess the significance of the substantial changes in the outer CN abundance distribution that follow from using the larger rate.

4.2. *Variations from the Standard Case*

4.2.1. *The interstellar UV Field*

IRC +10216 is likely to be closer than the Sun is to the main stellar sources in the Orion association, according to our simple geometric analysis of the respective distances of the two objects. Therefore, the average radiation field at IRC +10216 should be stronger than at the Sun, assuming there is no enhancement of the extinction along its line of sight. Thus, we consider a UV field that is 3 times larger than the Draine field. On the other hand, Martin & Rodgers (1987) deduced a substantially smaller field, which could arise from dust extinction along the line of sight to the illuminating stars. Thus, we also consider a variation in which the local UV radiation at IRC +10216 is decreased by a factor 3.

The spatial distributions of HCN and CN are shown in Figure 4 for the standard case and the two variations just discussed. As expected, the stronger field dissociates parent species deeper in the envelope than the weaker field. Factors of 3 variations in the radiation field lead to shifts in the positions in the CN peaks or the sizes of the HCN distributions by a factor of 1.4. At the standard distance, these changes are somewhat larger than the angular resolution of existing mm arrays. However, there are several ways that similar position shifts could be produced, for example, by changing the opacity of the envelope or reducing the distance by 25–50 pc.

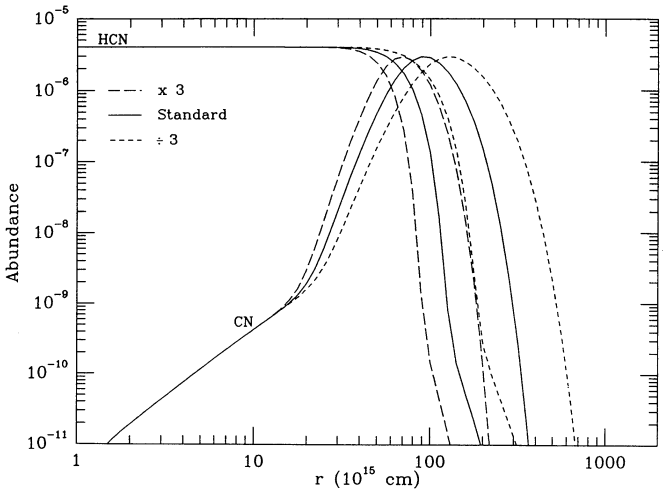

FIG. 4.—Variations in the HCN and CN abundances for the standard model and variations in the interstellar UV radiation field by overall factors of 3 larger and smaller.

4.2.2. *Dust Properties*

We illustrate the role of circumstellar dust opacity with AC dust particles of size $a = 100$ Å and 500 Å which, according to Figure 1 based on the work of Rouleau & Martin (1991), have very different extinction properties. The "large" particles show an almost constant UV extinction between 1100 and 1600 Å, where many of the important species are dissociated, whereas the extinction of "small" particles increases strongly with decreasing wavelength and can be described by a power law varying as λ^{-3} for 1000 Å $\leq \lambda \leq$ 1600 Å. Figure 5 gives the CN distribution for the dust extinction efficiencies illustrated in Figure 1.

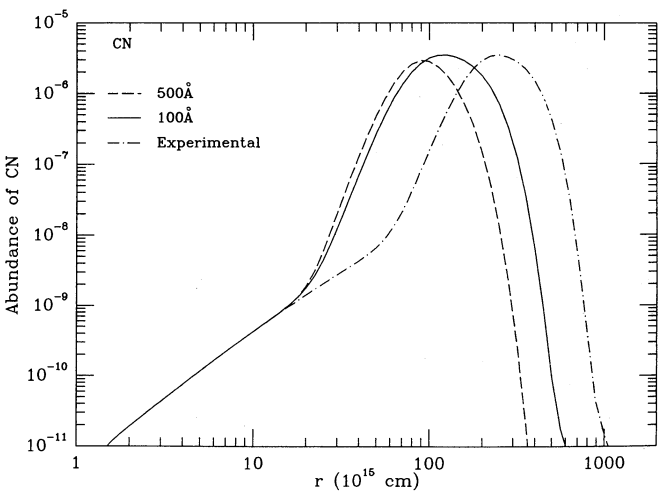

FIG. 5.—The CN abundance distributions for the dust models in Fig. 1

The "small" grains produce a somewhat more extended spatial distribution than the "large" grains, with the CN peak occurring at $\sim 1.2 \times 10^{17}$ cm (40″) instead of 9×10^{16} cm (30″). Even more envelope shielding is produced by the 40 Å mean-size grains obtained in the Colangeli et al. (1992) experiment, with the peak shifted out to $\sim 2.4 \times 10^{17}$ cm (80″). This last choice for the dust properties is unsatisfactory because the large shielding pushes many of the species distributions out to rather large radii. It also leads to very small abundances for HC_3N and other cyanopolyynes, and to a high HCO^+ abundance relative to the measurements, as discussed below in § 4.2.3.

We have adopted large dust grains ($a = 500$ Å) in our standard model because the resulting peak abundances of C_2H, CN, and HC_3N appear to be in better agreement with observations. This choice is also supported by the modeling of the IR emission flux of IRC +10216 by Martin & Rodgers (1987), with particles of one size ($a = 500$ Å), which agrees well with observations. Although we advocate 500 Å particles, we cannot really rule out the small 100 Å grains, or some distribution of sizes that peaks in this range, nor can we rule out some contribution from larger particles. However, it would not be surprising if the circumstellar dust in IRC +10216 were different from interstellar dust, which is believed to have a distribution in sizes from 50 to 2500 Å. Aside from the fundamental difference in chemical environment, circumstellar and interstellar dust have evolved differently. The dust grains in IRC +10216 are formed quite close to the photosphere (within $3R_*$ according to Danchi et al. 1990) by a mechanism likely to be strongly influenced by the shocks generated by the stellar pulsations (Bowen 1988). Then the dust is probably processed by interactions with the gas in the inner envelope for a period of the order of a few hundred years, certainly much shorter than the time available for interstellar dust to develop. This short evolutionary time may well play an important role in limiting the size distribution of circumstellar dust.

4.2.3. *Cosmic-Ray Ionization Rate*

Molecular synthesis by cosmic rays was discussed extensively by GLO and GMOL, particularly the molecular-ion progenitors of neutral species and the observability of "signature" ions such as HCO^+. At the time these papers were published, HCO^+ had not yet been detected in IRC +10216, and upper limits to the flux of the $J = 1$–0 transition were used in comparing theory and observations and in limiting the cosmic-ray ionization rate ζ. The models used for this purpose were also less complete and more phenomenological than the one described in this paper. Therefore, in view of the importance of making a definitive determination of the cosmic-ray ionization rate for IRC +10216, we reconsider the problem in this section: We first take up the case of HCO^+, which GLO emphasized as a test of ion-molecule chemistry, because it is produced mainly by proton-exchange with the fundamental cosmic-ray ion H_3^+. The flux of an optically thin HCO^+ rotational transition is proportional to ζ because the peak ion abundance is determined by the ratio of cosmic-ray production to neutral destruction by C_2H_2 and HCN.

Lucas & Guélin (1988) reported the detection of the $J = 1$–0 line of HCO^+ with the 30 m telescope, with a peak brightness temperature of about 20 mK. We can scale the brightness temperature calculations of GMOL to the smaller mass-loss rate used in the present paper and crudely correct for the larger peak and size of the HCO^+ abundance distribution for our standard model (both factor are about 65%). The resulting brightness temperature is ~40 mK, which is about twice as large as the observational result. If our purpose were to fine-tune the model, a smaller value could easily be obtained by varying the model parameters, particularly reducing the far-UV envelope opacity. Because of the great sensitivity of the HCO^+ peak abundance to the cosmic-ray ionization rate, however, values of ζ for IRC +10216 much larger than the value used in the standard model ($\zeta = 5 \times 10^{-18}$ s^{-1}) would be difficult to reconcile with the HCO^+ detection reported by Lucas & Guélin (1988).

This conclusion is to be contrasted with the result of modeling diffuse interstellar clouds (e.g., van Dishoeck & Black 1986; Viala 1986), who find that $\zeta \approx 5 \times 10^{-17}$ s^{-1} for a group of clouds observed in depth by absorption-line spectroscopy against early-type stars. This finding is strongly based on the OH radical, whose abundance depends on that of H_3^+ because OH is produced in part by the ion-molecule reaction, $H_3^+ + O \rightarrow OH^+ + H_2$. If the rate coefficient for the dissociative recombination of H_3^+ has the traditional, large value, for example, as indicated by the recent measurements of Amano (1990), the cosmic-ray ionization rate deduced from observations of diffuse clouds would have to be increased by a substantial factor ~10 (van Dishoeck & Black 1986), that is, two orders of magnitude larger than the value used for IRC +10216.

A large cosmic-ray ionization rate would have other observational consequences for IRC +10216, as suggested by the HC_3N abundance shown in Figure 6 for a tenfold increase in ζ relative to the standard case. We find that increasing ζ by 10 has the following additional consequences: (1) Although the HC_3N peak is increased by only ~25%, the abundance in the inner envelope is larger by a factor of 10, enough to be measured by interferometric observations. We have already discussed in § 3 other ways of filling in the interior of the HC_3N shell, that is, by injection from the near-stellar regions or by increasing the branching of the dissociative recombination of H_2CN^+ toward CN, Reaction 56. (2) The increase in interior HC_3N is caused by the combined effects of ion-molecule and neutral reactions. The H_2CN^+ abundance is increased by a factor of 3, because the ion is both produced and destroyed by cosmic-ray processes, at least before the peak. The increased abundance of H_2CN^+ then leads to a large increase in interior CN and thus of HC_3N via Reaction 199. (3) The interior abun-

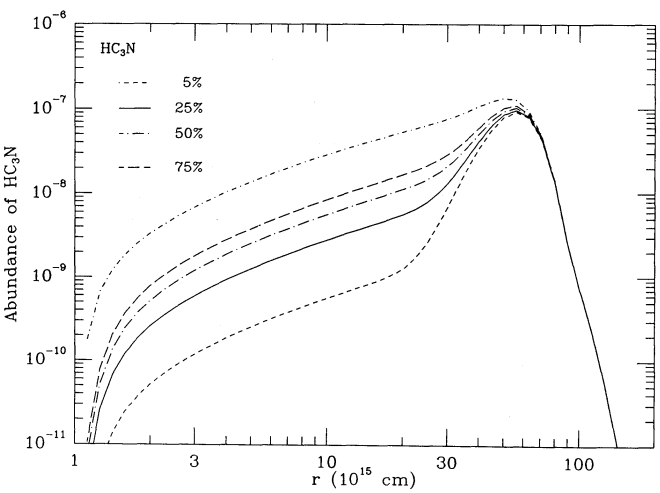

FIG. 6.—The HC_3N abundance for different values of the branching ratio b in Reaction 56, $H_2CN^+ + e^- \rightarrow CN + H_2$. Also shown, the HC_3N abundance for the cosmic-ray rate $\zeta = 5 \times 10^{-17}$ s^{-1}. The solid curve is the standard model.

dance of HNC is also raised by 10 and the peak abundance by 4; the location of the peak has moved in toward smaller radii by about 25%. These changes are again largely due to the increased abundance of H_2CN^+, the main progenitor of HNC. The observations of HNC in IRC +10216 were duscussed at some length by GMOL, who concluded that the relatively large observed ratio HNC/$H^{13}CN$ ($\sim\frac{1}{7}$) could be accounted for by ion-molecule reactions with the same value of ζ used in the present standard model. As already emphasized by GMOL, increasing ζ by a factor of 10 would destroy this good agreement.

To summarize, application of standard cosmic-ray-induced, ion-molecule reaction processes to IRC +10216 offers several independent methods for determining the cosmic-ray ionization rate for this star. The two most direct ways involve HCO^+ and HNC and both suggest that large increases in ζ above the value used in our standard model are ruled out. We remark that we do *not* expect the cosmic-ray ionization rate to be larger than the value, $\zeta = 5 \times 10^{-18}$ s^{-1}, used here and in previous versions of the model. It was originally chosen to correspond to high-energy (>GeV) cosmic rays (Spitzer & Tomasko 1962; Nakano & Tademaru 1972). The larger value for diffuse clouds presumably comes from low-energy cosmic rays, which are likely to be magnetically excluded from the relatively high-density circumstellar envelope of IRC +10216 (J. Bieging 1992, private communication; Tielens 1992).

4.3. *The Cyanopolyyne Abundances*

The spatial distributions of the cyanopolyynes predicted by the photochemical model (Fig. 3) all show prominent peaks in the range 4–8 $\times$ 10^{16} cm, or 15″–25″ for the nominal distance of 200 pc. The distribution of HC_3N is special in that it has a broad shoulder at smaller distances, $r \leq 3 \times 10^{16}$ cm, or 10″, which we will discuss in detail below. The peaks shifted slightly toward larger radii as the molecules become more complex. The photoproduced radicals are shifted with respect to their parents by larger amounts, $\sim$3″, an effect that might be observable with large telescopes. The spatial distribution of the brightness of the lines is also affected by excitation processes, and a careful analysis of several lines is required to confirm this prediction. The best case for study is the HC_3N–C_3N pair since C_5N is probably not susceptible to detailed study because of its small dipole moment (Pauzat, Ellinger, & Mclean 1992); moreover its radio-frequency spectrum has not yet been measured.

There is considerable observational evidence that HC_3N has a peaked spatial distribution in IRC +10216. Most dramatically, Bieging & Rieu (1988) analyzed a one-line interferometer map of the molecule, using a prescribed excitation temperature distribution, and derived a shell distribution with a peak abundance of 2×10^{-7} (after correction to our mass-loss rate) at $r = 4.5 \times 10^{16}$ cm; the uncertainty in the abundance is estimated to be at least a factor of 3. They also observed HC_3N in the interior of the shell ($r < 10^{16}$ cm) with an abundance of 3×10^{-8}. The peak theoretical HC_3N abundance in Figure 2 is 10^{-7}, which is in good agreement with the observations considering the uncertainties. The theoretical peak position occurs at $r = 6 \times 10^{16}$ cm, which is larger than the position given by Bieging & Rieu (1988) by a factor 1.4. Again considering the preliminary and uncertain nature of the observations and the many variables entering the theory, it would be premature to take this difference very seriously.

Two types of chemical processes have been suggested for the formation of HC_3N in the envelope of IRC +10216, ion-molecule and neutral reactions. Near the peak, the neutral Reaction 199 dominates over the ionic Reactions 158 and 159 by a factor of 20, confirming the conclusion of Howe & Millar (1990), when the cosmic-ray ionization rate is $\zeta = 5 \times 10^{-18}$ s^{-1}. It is important to emphasize that both processes are photochemical in origin, that is, the high-energy activators, CN and $C_2H_2^+$, are produced radiatively.

In the inner part of the envelope, the CN radical is produced by dissociative recombination of the molecular ion, H_2CN^+, Reaction 56. This process produces HCN and HNC as well as CN, but none of the branching ratios have been measured. For the standard case, we use the value b(CN) = 0.25, and we show in Figure 6 how the HC_3N abundance changes with b. Increasing the branching ratio from 0.25 to 0.75 enhances the HC_3N production in the inner envelope by a factor $\sim$4. Being closer to the star, the inner molecules are more easily excited, and this may account for the observation of HC_3N interior to shell. An additional potential contributor in this region is HC_3N formed under thermal equilibrium conditions in the upper atmosphere of the star, if it survives passage through the region of dust formation. Any HC_3N injected into the outer envelope will produce an abundance distribution that is constant throughout the envelope, at least until the neighborhood of the peak is approached. It would be of great interest to analyze the spectral maps of HC_3N in several lines, now being prepared at IRAM (M. Guélin & C. Kahane 1991, private communication), with a view of testing the theoretical distributions of HC_3N shown in Figures 3 and 6.

The ratio of the peak abundances of HC_3N and C_3N is $\sim$3 for the standard model, in reasonable agreement with the column density ratio of 2 given by Cernicharo et al. (1987). Earlier photochemical models tended to yield a ratio of the order unity. The new element in the present calculations is Reaction 204 which is now an important destruction process for C_3N.

The prospects for understanding the larger cyanopolyynes in the context of the photochemical model are not as favorable as they are for HC_3N and C_3N, where the results so far are quite promising. Except for HC_5N, it is unlikely that observations of comparable detail will be available soon because the strengths of the mm lines becomes progressively weaker with mass. We have already mentioned the special problem with the radical C_5N. The higher order cyanopolyynes, HC_iN for i = 5, 7, 9, 11, have been detected at cm wavelengths and, in some cases, mapped with the VLA. Nonetheless, the prospects for making spectral maps in two or more lines, differing sufficiently in excitation energy to determine both the abundance and the excitation as a function of distance, seem poor except for HC_5N and possibly HC_7N.

At the present time, we have little to go on except for beam-averaged column densities derived by taking both the abundance and the excitation temperature constant in the envelope, both rather unrealistic assumptions. The conclusion from such analyses is that the cyanopolyyne abundance decreases by roughly a factor of 3 when two (triply bonded) carbons are added (Cernicharo et al. 1987). Our model calculations give much larger decrements in peak abundances, for example, $HC_3N/HC_5N \sim 25$ and $HC_5N/HC_7N \sim 10$. Although the new chemical route described by Reactions 204 and 205 contributes 50% of the total production of large cyanopolyynes and thereby represents a promising mechanism to consider, the neutral reaction pathways to HC_5N and HC_7N (Reactions 200–201 and 204–205) appear to be too weak to explain the decrements presented by Cernicharo et al. (1987). None of the rate coefficients for these reactions have been measured, and it is unlikely that we have underestimated their values in Appendix B by an order of magnitude. Some other process must be

responsible for the production of the larger cyanopolyynes in IRC +10216. Jura & Kroto (1990) have suggested that HC_7N in AFGL 2688 could form from grain-grain collisions in the bipolar outflow, but it is unclear how to implement this suggestion for IRC +10216, which is a more quiescent and spherical envelope.

4.4. *The Allenic Radical* HCCN

In their discovery paper, Guélin & Cernicharo (1991) derive a beam-averaged column density for HC_2N of 1.3×10^{13} cm^2, or 200 times smaller than that for HC_3N. They also give upper limits for the column densities of H_2C_2N and C_2N that are 3 and 5 times larger. Assuming Reactions 186 and 62 are the major routes to HC_2N formation, the photochemical model predicts shell distributions for these three related species that are in good accord with the estimates of Guélin & Cernicharo. For our standard case, the peak abundances obtained for HC_2N, C_2N, and H_2C_2N are 6×10^{-10}, 1.2×10^{-9}, and 3.2×10^{-10}, respectively. Because the HC_3N and HC_2N peaks are at about the same position, it is appropriate to compare their peak abundances, and our ratio is 167, essentially the same as observed. The peak abundances of C_2N, and H_2C_2N are also consistent with the upper limits of Guélin & Cernicharo. Hence, the presence of HC_2N in IRC +10216 can be explained by the same chemical pathway proposed for molecular clouds (Irvine et al. 1988).

After the manuscript was submitted for publication, we received a preprint from Bieging & Tafalla (1992) reporting interferometric observations of HC_3N and C_3N in IRC +10216 that are relevant for the results of this section. With an angular resolution of 7″, these authors find shell distributions characteristic of the photochemical model. For the case of HC_3N, they determine that the abundance peak 3.5×10^{-7} (relative to total hydrogen) occurs at $r = 2.35 \times 10^{16}$ cm for their choice of distance, $d = 100$ pc. The abundance decreases rapidly toward the center, being consistent with nearly zero intensity observed on the star. If we translate the results of Figure 3 using this distance, the theoretical peak occurs at 2.8×10^{16} cm, about 20% larger than given by Bieging & Tafalla. However, our mass-loss rate is 50% larger, so when an appropriate correction is made for the shift inwards of the peaks (the peak position varies roughly as $\dot{M}^{0.5}$), the theoretical and observational peak positions agree. The theoretical peak abundance in Figure 3 is about one third of the value given by Bieging & Tafalla, which is acceptable considering the many uncertainties. The C_3N distribution is similar to HC_3N, but is larger in spatial extension. Its peak is shifted out by about 5″, and the peak level is reduced by 2.5 compared to HC_3N. The displacement and the relative heights of the two distributions are similar to those given by the theory in Figure 3.

5. CONCLUSION

The photochemical model presented in this paper is considerably improved with respect to earlier versions, such as GLO and GMOL. Major changes have been made in the treatment of photodissociation and in dust and molecular shielding, thereby avoiding in large part the previous phenomenological approach. The chemistry has also been updated and extended. This results in a model that can be used to interpret spectral maps of nearby circumstellar envelopes and to deduce their physical and chemical properties. Thus our calculations of the spatial distribution of the main observed species (HCN, CN, C_2H, and HC_3N) provide insight into the nature of the circumstellar dust in IRC +10216 and on the character of the chemistry that is active in the outer envelope. For example, our standard model employs AC particles with an average size ~500 Å, in accord with the modeling of the infrared continuum by Martin & Rodgers (1987).

Turning to the problem of the cyanopolyynes, our model seems able to account for the available information on HC_3N and C_3N in IRC +10216. Neutral radical reactions dominate the ion-molecule pathways considered by GLO and GMOL, largely as a result of the small cosmic-ray ionization rate associated with high-energy cosmic rays and supported by the measured abundance of HCO^+. Although the model predicts that the abundances of the larger cyanopolyynes decrease with molecular weight, it does not reproduce the quantitative sequence given by Cernicharo et al. (1987). Both improved chemical models and observations are needed to make further progress on this problem.

The theory is still limited by the paucity of laboratory data on photodissociation cross sections and on chemical reactions. An important improvement in the photochemical model is the inclusion of a temperature variation for the radical-molecule reactions responsible for forming the cyanopolyynes. A weak, inverse temperature dependence is suggested by theory (e.g. Clary 1985; Stoecklin, Dateo, & Clary 1991) and has been recently measured at low temperatures for the CN radical reaction, $CN + O_2 \rightarrow CNO + O$ (Rowe, Canosa, & Sims 1993). This type of temperature variation suggests that neutral-neutral reactions have larger rate coefficients at the low gas temperatures characteristic of the outer envelope of IRC +10216 than at room temperature. Preliminary results on the effect of such enhanced rate coefficients on the abundances of the cyanopolyyne and small hydrocarbon molecules are promising and will be reported in another publication.

Additional basic improvements in the photochemical model are also needed. For example, incorporation of clumping could provide part of the answer to the deficiency of the higher order cyanopolyynes, characteristic of the present model, by enhancing the efficiency of the neutral chemistry. Although we have significantly improved the radiative transfer, the inclusion of dust scattering might result in slightly smaller spatial distributions. Although IRC +10216 is the best-studied circumstellar envelope, our knowledge of the spatial distribution of the most important circumstellar molecules is still quite limited. The set of molecules which could be spectrally mapped for this source in more than one line at mm wavelengths and thereby provide tests of the photochemical model consists of the following species: C_2H, HCN, HNC, CN, HC_3N, C_3N, and HC_5N, not to mention particular silicon and sulfur molecules not discussed in the present work. Significant progress has already been made to carry out this program with large mm telescopes and interferometers (see, e.g., Lucas 1992). We believe that the analysis of such data with the improved photochemical model presented here will provide interesting new information on the physical and chemical properties of the prototypical C-rich circumstellar envelope of IRC +10216.

The authors would like to thank P. G. Martin for carrying out special calculations of the optical properties of small AC grains. We are also grateful to A. Dalgarno for remarking that a large H_3^+ dissociation rate implies a large cosmic-ray ionization determined from diffuse interstellar clouds. We also wish to thank J. H. Bieging for a critical review of the manuscript, for providing a preprint on recent interferometric observations, and for help in clarifying the discussion on the cosmic-ray ionization rate in § 4.2.3. This research has been supported in part by NASA's program in infrared, submillimeter, and radio astronomy through grant NAGW-630.

APPENDIX A

PHOTODISSOCIATION RATES[a]

Number	Reaction	Rates (s^{-1}) Bands[b] 1	2	3	4	5	6	References[c]
1	$C_2H_2 \rightarrow C_2H + H$	2.1 (−10)	1.3 (−9)	1.1 (−9)	3.3 (−10)	2.5 (−11)	1.7 (−12)	1, E
2	$C_2H_2 \rightarrow C_2H_2^+ + e^-$	3.3 (−10)						1, E
3	$C_2H \rightarrow C_2 + H$	9.1 (−11)	1.7 (−10)	1.8 (−10)	7.5 (−11)			2, T
4	$C_2H \rightarrow C_2H^+ + e^-$	3 (−11)						Estimated
5	$CH \rightarrow C + H$	9.5 (−10)						2
6	$CH \rightarrow CH^+ + e^-$	7.5 (−10)						2
7	$CH_2 \rightarrow CH + H$	7.2 (−10)						2
8	$C_2 \rightarrow C + C$	7.2 (−11)	6.9 (−11)					3, T
9	$C_2 \rightarrow C_2^+ + e^-$	2.1 (−10)						3, T
10	$C \rightarrow C^+ + e^-$	3.3 (−10)						2
11	$C_2H_3 \rightarrow C_2H_2 + H$	2.2 (−9)						Estimated
12	$C_3 \rightarrow C_2 + C$	3.8 (−9)						2
13	$C_3H \rightarrow C_3 + H$	4.5 (−10)						Estimated
14	$C_3H \rightarrow C_2H + C$	1.5 (−10)						Estimated
15	$C_3H \rightarrow CH + C + C$	1.5 (−10)						Estimated
16	$cC_3H_2 \rightarrow C_3H + H$	9.9 (−10)						2
17	$cC_3H_2 \rightarrow C_3 + 2H$	9.9 (−10)						2
18	$lC_3H_2 \rightarrow C_3H + H$	9.9 (−10)						R16
19	$lC_3H_2 \rightarrow C_2H + CH$	6.6 (−10)						Estimated
20	$C_4 \rightarrow C_2 + C_2$	2 (−10)						4
21	$C_4 \rightarrow C_3 + C$	2 (−10)						4
22	$C_4H \rightarrow C_4 + H$	3.9 (−10)						Estimated
23	$C_4H \rightarrow C_2H + C_2$	9.9 (−11)						Estimated
24	$C_4H_2 \rightarrow C_4H + H$	1.9 (−9)						5
25	$C_4H_2 \rightarrow C_2H + C_2H$	1.9 (−9)						R24
26	$C_4H_2 \rightarrow C_4H_2^+ + e^-$	4.5 (−10)						5
27	$C_5 \rightarrow C_4 + C$	2.9 (−9)						Estimated
28	$C_5 \rightarrow C_3 + C_2$	9.9 (−10)						Estimated
29	$C_5H \rightarrow C_5 + H$	4.5 (−10)						Estimated
30	$C_5H \rightarrow C_3H + C_2$	7.8 (−11)						Estimated
31	$C_5H \rightarrow C_2H + C_3$	7.8 (−10)						Estimated
32	$C_5H_2 \rightarrow C_5H + H$	9.9 (−10)						R16
33	$C_5H_2 \rightarrow C_3H + C_2H$	6.6 (−10)						R19
34	$C_5H_3 \rightarrow C_5H_2 + H$	9.9 (−10)						R16
35	$C_5H_4 \rightarrow C_5H_3 + H$	3.3 (−9)						5
36	$HCN \rightarrow CN + H$	4.1 (−10)	8.7 (−10)	1.1 (−10)	2.9 (−12)			6, E
37	$CN \rightarrow C + N$	2 (−10)						9
38	$HNC \rightarrow CN + H$	1.5 (−9)						R36
39	$HC_2N \rightarrow C_2N + H$	1.7 (−9)						Estimated
40	$HC_2N \rightarrow CH + CN$	1.7 (−9)						Estimated
41	$HC_2N \rightarrow C_2H + N$	1.7 (−9)						Estimated
42	$H_2C_2N \rightarrow HC_2N + H$	1.7 (−9)						Estimated
43	$H_2C_2N \rightarrow C_2N + 2H$	1.7 (−9)						Estimated
44	$H_2C_2N \rightarrow CN + CH_2$	1.7 (−9)						Estimated
45	$C_2N \rightarrow CN + C$	1.7 (−9)						Estimated
46	$CO \rightarrow C + O$	1 (−10)						7
47	$HC_3N \rightarrow C_3N + H$	1 (−10)	4.9 (−10)	1.2 (−9)	1 (−10)			8
48	$HC_3N \rightarrow C_2H + CN$	2 (−10)	9.8 (−10)	2.4 (−9)	2 (−10)			8
49	$C_3N \rightarrow C_2 + CN$	2 (−10)	9.8 (−10)	2.4 (−9)	2 (−10)			R48
50	$HC_5N \rightarrow C_5N + H$	1 (−10)	4.9 (−10)	1.2 (−9)	1 (−10)			R47
51	$HC_5N \rightarrow C_4H + CN$	1 (−10)	4.9 (−10)	1.2 (−9)	1 (−10)			R47
52	$HC_5N \rightarrow C_2H + C_3N$	1 (−10)	4.9 (−10)	1.2 (−9)	1 (−10)			R47
53	$C_5N \rightarrow C_4 + CN$	1 (−10)	4.9 (−10)	1.2 (−9)	1 (−10)			R47
54	$C_5N \rightarrow C_2 + C_3N$	1 (−10)	4.9 (−10)	1.2 (−9)	1 (−10)			R47
55	$HC_7 \rightarrow C_7N + H$	1 (−10)	4.9 (−10)	1.2 (−9)	1 (−10)			R47
56	$HC_7N \rightarrow C_2H + C_5N$	6.4 (−11)	3.1 (−10)	7.6 (−10)	6.5 (−11)			Estimated
57	$HC_7N \rightarrow C_4H + C_3N$	6.4 (−11)	3.1 (−10)	7.6 (−10)	6.5 (−11)			R56
58	$HC_7N \rightarrow C_6H + CN$	6.4 (−11)	3.1 (−10)	7.6 (−10)	6.5 (−11)			R56
59	$C_7N \rightarrow C_6 + CN$	6.4 (−11)	3.1 (−10)	7.6 (−10)	6.5 (−11)			R56
60	$C_7N \rightarrow C_4 + C_3N$	6.4 (−11)	3.1 (−10)	7.6 (−10)	6.5 (−11)			R56
61	$C_7N \rightarrow C_2 + C_5N$	6.4 (−11)	3.1 (−10)	7.6 (−10)	6.5 (−11)			R56
62	$N_2 \rightarrow N + N$	2.3 (−10)	...	...	...			2

[a] Rates calculated for the mean interstellar radiation as determined by Draine 1978.

[b] The photodissociation rates are distributed over six wavelength bands: 1 = [910–1100 Å], 2 = [1100–1300 Å], 3 = [1300–1500 Å], 4 = [1500–1700 Å], 5 = [1700–1900 Å], 6 = [1900–2100 Å].

[c] E and T indicate, respectively, whether the rates have been calculated from experimental or theoretical cross sections; "estimated" means that the rates are either the latest theoretical estimates available in the literature or "educated" guesses. "R*n*" refers to the reaction number.

(1) Cross sections measured by Nakayama & Watanabe 1964, Suto & Lee 1984, Wu & Judge 1985, Wu et al. 1989, and Smith et al. 1991.
(2) van Dishoeck 1988.
(3) Cross sections estimated by Pouilly et al. 1983.
(4) Herbst & Leung 1986.
(5) Roberge et al. 1991.
(6) Cross sections measured by Lee 1980.
(7) Glassgold et al. 1987.
(8) Total rate from van Dishoeck 1988 distributed over the whole bands following the cross sections from Connors et al. 1974.
(9) Total rate from van Dishoeck 1988, with the wavelength dependence given by Lavendy et al. 1987.

APPENDIX B

CHEMICAL REACTIONS

Number	Reaction	Rate Coefficient[a] A	n	References[b]
	Dissociative Recombination			
1	$C^+ + e^- \rightarrow C$	4.1 (−10)	0.9	1
2	$CH^+ + e^- \rightarrow C + H$	1.6 (−6)	0.42	2
3	$CH_2^+ + e^- \rightarrow CH + H$	2.2 (−6)	0.5	2
4	$CH_2^+ + e^- \rightarrow C + H + H$	2.2 (−6)	0.5	2
5	$CH_3^+ + e^- \rightarrow CH_2 + H$	2 (−6)	0.5	2
6	$CH_3^+ + e^- \rightarrow CH + H + H$	2 (−6)	0.5	2
7	$CH_3^+ + e^- \rightarrow C + H + H + H$	2 (−6)	0.5	2
8	$C_2H^+ + e^- \rightarrow C_2 + H$	2.8 (−6)	0.5	2
9	$C_2H^+ + e^- \rightarrow CH + C$	1.9 (−6)	0.5	2
10	$C_2^+ + e^- \rightarrow C + C$	5.2 (−6)	0.5	2
11	$C_2H_2^+ + e^- \rightarrow C_2H + H$	2.8 (−6)	0.5	2
12	$C_2H_2^+ + e^- \rightarrow C_2 + H + H$	1.9 (−6)	0.5	2
13	$C_2H_3^+ + e^- \rightarrow C_2H_2 + H$	4.7 (−6)	0.5	2
14	$C_2H_3^+ + e^- \rightarrow C_2H + H + H$	1.6 (−6)	0.5	2
15	$C_2H_3^+ + e^- \rightarrow C_2 + H + H + H$	1.6 (−6)	0.5	2
16	$C_2H_4^+ + e^- \rightarrow C_2H_3 + H$	4.7 (−6)	0.5	R13
17	$C_2H_4^+ + e^- \rightarrow C_2H_2 + H + H$	3.1 (−6)	0.5	R14 + R15
18	$C_3^+ + e^- \rightarrow C_2 + C$	5.2 (−6)	0.5	R10
19	$C_3H^+ + e^- \rightarrow C_3 + H$	3.1 (−6)	0.5	Estimated
20	$C_3H^+ + e^- \rightarrow C_2H + C$	2.1 (−6)	0.5	Estimated
21	$cC_3H_2^+ + e^- \rightarrow C_3H + H$	1 (−6)	0.5	Estimated
22	$cC_3H_2^+ + e^- \rightarrow C_3 + H + H$	6.9 (−7)	0.5	Estimated
23	$lC_3H_2^+ + e^- \rightarrow C_3H + H$	1 (−6)	0.5	R21
24	$lC_3H_2^+ + e^- \rightarrow C_3 + H + H$	6.9 (−7)	0.5	R22
25	$lC_3H_3^+ + e^- \rightarrow lC_3H_2 + H$	1 (−6)	0.5	R21
26	$lC_3H_3^+ + e^- \rightarrow C_3H + H + H$	3.5 (−6)	0.5	Estimated
27	$lC_3H_3^+ + e^- \rightarrow C_3 + H + H + H$	3.5 (−6)	0.5	Estimated
28	$cC_3H_3^+ + e^- \rightarrow cC_3H_2 + H$	1 (−6)	0.5	R25
29	$cC_3H_3^+ + e^- \rightarrow C_3H + H + H$	3.5 (−7)	0.5	R26
30	$cC_3H_3^+ + e^- \rightarrow C_3 + H + H + H$	3.5 (−7)	0.5	R27
31	$C_4H^+ + e^- \rightarrow C_4 + H$	3.1 (−6)	0.5	R19
32	$C_4H^+ + e^- \rightarrow C_2H + C_2$	2.1 (−6)	0.5	R20
33	$C_4H_2^+ + e^- \rightarrow C_4H + H$	6.4 (−6)	0.5	Estimated
34	$C_4H_2^+ + e^- \rightarrow C_2H + C_2H$	2.1 (−6)	0.5	Estimated
35	$C_4H_2^+ + e^- \rightarrow C_4 + H + H$	2.1 (−6)	0.5	Estimated
36	$C_4H_3^+ + e^- \rightarrow C_4H_2 + H$	6.4 (−6)	0.5	R34
37	$C_4H_3^+ + e^- \rightarrow C_2H + C_2H_2$	2.1 (−6)	0.5	R35
38	$C_4H_3^+ + e^- \rightarrow C_4H + H + H$	1.1 (−6)	0.5	Estimated
39	$C_4H_3^+ + e^- \rightarrow C_4 + H + H + H$	1.1 (−6)	0.5	Estimated
40	$C_5H^+ + e^- \rightarrow C_5 + H$	3.1 (−6)	0.5	R19
41	$C_5H^+ + e^- \rightarrow C_2H + C_3H$	2.1 (−6)	0.5	R20
42	$C_5H_2^+ + e^- \rightarrow C_5H + H$	1 (−6)	0.5	R21
43	$C_5H_2^+ + e^- \rightarrow C_5 + H + H$	6.9 (−7)	0.5	R22
44	$C_5H_3^+ + e^- \rightarrow C_5H_2 + H$	1 (−6)	0.5	R25
45	$C_5H_3^+ + e^- \rightarrow C_5H + H + H$	3.5 (−7)	0.5	R26
46	$C_5H_3^+ + e^- \rightarrow C_5 + H + H + H$	3.5 (−7)	0.5	R27
47	$C_5H_4^+ + e^- \rightarrow C_5H_3 + H$	1 (−6)	0.5	R21
48	$C_5H_4^+ + e^- \rightarrow C_5H_2 + H + H$	6.9 (−7)	0.5	R22
49	$C_5H_5^+ + e^- \rightarrow C_5H_4 + H$	3.6 (−6)	0.5	Estimated
50	$C_5H_5^+ + e^- \rightarrow C_5H_3 + H + H$	1.2 (−6)	0.5	Estimated
51	$C_5H_5^+ + e^- \rightarrow C_5H_2 + H + H + H$	1.2 (−6)	0.5	Estimated
52	$H_3^+ + e^- \rightarrow H_2 + H$	2.7 (−5)	0.9	8
53	$HCO^+ + e^- \rightarrow CO + H$	1.2 (−5)	0.65	8
54	$H_2CN^+ + e^- \rightarrow HCN + H$	2.3 (−6)	0.5	2
55	$H_2CN^+ + e^- \rightarrow HNC + H$	2.3 (−6)	0.5	2
56	$H_2CN^+ + e^- \rightarrow CN + H_2$	1.5 (−6)	0.5	2
57	$CNC^+ + e^- \rightarrow CN + C$	5.2 (−6)	0.5	3
58	$HCN^+ + e^- \rightarrow CN + H$	3.5 (−6)	0.5	3
59	$H_2C_2N^+ + e^- \rightarrow HC_2N + H$	2.3 (−6)	0.5	R54
60	$H_2C_2N^+ + e^- \rightarrow C_2N + H + H$	2.3 (−6)	0.5	R54
61	$H_3C_2N^+ + e^- \rightarrow H_2C_2N + H$	2.3 (−6)	0.5	R54
62	$H_3C_2N^+ + e^- \rightarrow HC_2N + H + H$	2.3 (−6)	0.5	R54
63	$H_4C_2N^+ + e^- \rightarrow H_2C_2N + H + H$	2.3 (−6)	0.5	R54
64	$H_2C_3N^+ + e^- \rightarrow HC_3N + H$	7 (−6)	0.5	Estimated
65	$H_2C_3N^+ + e^- \rightarrow C_3N + H + H$	4 (−6)	0.5	Estimated
66	$H_2C_3N^+ + e^- \rightarrow CN + C_2H_2$	4 (−6)	0.5	Estimated
67	$H_2C_5N^+ + e^- \rightarrow HC_5N + H$	5 (−6)	0.5	Estimated
68	$H_2C_5N^+ + e^- \rightarrow C_5N + H + H$	4 (−6)	0.5	Estimated
69	$H_2C_5N^+ + e^- \rightarrow C_3N + C_2H_2$	3 (−6)	0.5	Estimated

APPENDIX B—*Continued*

Number	Reaction	Rate Coefficient[a] A	n	References[b]
70	$H_2C_5N^+ + e^- \rightarrow CN + C_4H_2$	3 (−6)	0.5	Estimated
71	$H_3C_5N^+ + e^- \rightarrow HC_5N + H + H$	5 (−6)	0.5	R67
72	$H_3C_5N^+ + e^- \rightarrow C_5N + H + H + H$	4 (−6)	0.5	R68
73	$H_3C_5N^+ + e^- \rightarrow HCN + C_4H_2$	3 (−6)	0.5	R70
74	$H_3C_5N^+ + e^- \rightarrow HC_3N + C_2H_2$	3 (−6)	0.5	R69
75	$H_2C_7N^+ + e^- \rightarrow HC_7N + H$	5 (−6)	0.5	Estimated
76	$H_2C_7N^+ + e^- \rightarrow C_7N + H + H$	4 (−6)	0.5	Estimated
77	$H_2C_7N^+ + e^- \rightarrow C_5N + C_2H_2$	2 (−6)	0.5	Estimated
78	$H_2C_7N^+ + e^- \rightarrow C_3N + C_4H_2$	2 (−6)	0.5	Estimated
79	$H_2C_7N^+ + e^- \rightarrow CN + C_6H_2$	2 (−6)	0.5	Estimated
80	$H_3C_7N^+ + e^- \rightarrow HC_7N + H + H$	5 (−6)	0.5	R75
81	$H_3C_7N^+ + e^- \rightarrow C_7N + H + H + H$	4 (−6)	0.5	R76
82	$H_3C_7N^+ + e^- \rightarrow HCN + C_6H_2$	2 (−6)	0.5	R79
83	$H_3C_7N^+ + e^- \rightarrow HC_3N + C_4H_2$	2 (−6)	0.5	R78
84	$H_3C_7N^+ + e^- \rightarrow HC_5N + C_2H_2$	2 (−6)	0.5	R77
85	$C_4N^+ + e^- \rightarrow CN + C_3$	2.6 (−6)	0.5	3
86	$C_4N^+ + e^- \rightarrow C_3N + C$	2.6 (−6)	0.5	3
87	$N_2H^+ + e^- \rightarrow N_2 + H$	2.2 (−5)	0.73	8
88	$N_2H^+ + e^- \rightarrow N + N + H$	2.2 (−5)	0.73	8
	Ion-Molecule Reactions			
89	$CH^+ + H_2 \rightarrow CH_2^+ + H$	1.2 (−9)	...	4
90	$CH^+ + HCN \rightarrow H_2CN^+ + C$	7.3 (−8)	0.65	4
91	$CH^+ + HCN \rightarrow CNC^+ + H + H$	1.5 (−8)	0.65	4
92	$CH^+ + HCN \rightarrow HC_2N^+ + H$	9.8 (−9)	0.65	4
93	$CH + + C_2H_2 \rightarrow lC_3H_2^+ + H$	2.4 (−9)	...	4
94	$CH_2^+ + HCN \rightarrow H_2C_2N^+ + H$	7.3 (−8)	0.65	4
95	$CH_2^+ + HC_3N \rightarrow H_2C_3N^+ + CH$	1.7 (−7)	0.65	4
96	$CH_2^+ + H_2 \rightarrow CH_3^+ + H$	1.6 (−9)	...	4
97	$CH_2^+ + C_2H_2 \rightarrow lC_3H_3^+ + H$	2.5 (−9)	...	4
98	$CH_3^+ + HCN \rightarrow H_4C_2N^+ + h\nu$	6.9 (−8)	0.65	4
99	$CH_3^+ + HC_3N \rightarrow lC_4H_3^+ + HCN$	1.7 (−7)	0.65	4
100	$CH_3^+ + C_2H_2 \rightarrow lC_3H_3^+ + H_2$	1.2 (−9)	...	4
101	$C^+ + C_2H_2 \rightarrow C_3H^+ + H$	2.8 (−9)	...	4
102	$C^+ + C_2H \rightarrow C_3^+ + H$	4.1 (−8)	0.65	3
103	$C_2^+ + H_2 \rightarrow C_2H^+ + H$	1.2 (−9)	...	11
104	$C_2H^+ + H_2 \rightarrow C_2H_2^+ + H$	1.7 (−9)	...	4
105	$C_3H^+ + H_2 \rightarrow cC_3H_2^+ + H$	5.2 (−12)	...	4
106	$C_3H^+ + H_2 \rightarrow cC_3H_3 + h\nu$	8.6 (−10)	0.65	4
107	$C_3H^+ + H_2 \rightarrow lC_3H_3 + h\nu$	5.7 (−9)	0.65	4
108	$C_3H^+ + C_2H_2 \rightarrow C_2H_2^+ + H$	5.7 (−10)	...	4
109	$C_3H^+ + C_4H_2 \rightarrow C_7H_2^+ + H$	3.4 (−10)	...	Estimated
110	$C_3H^+ + C_4H_2 \rightarrow C_5H_2^+ + C_2H$	2.3 (−10)	...	Estimated
111	$cC_3H_2^+ + C_2H_2 \rightarrow C_5H_3^+ + H$	1.1 (−9)	...	11
112	$lC_3H_2^+ + C_2H_2 \rightarrow C_5H_3^+ + H$	9 (−10)	...	11
113	$cC_3H_3^+ + C_2H_2 \rightarrow C_5H_3^+ + H_2$	1.1 (−9)	...	11
114	$C_3^+ + H_2 \rightarrow C_3H^+ + H$	1.7 (−10)	...	11
115	$C^+ + HCN \rightarrow CNC^+ + H$	1.2 (−7)	0.65	11
116	$C^+ + HNC \rightarrow CNC^+ + H$	1.2 (−7)	0.65	R115
117	$C^+ + HC_3N \rightarrow C_3H^+ + CN$	1.3 (−7)	0.65	4
118	$C^+ + HC_3N \rightarrow C_4N^+ + H$	5.7 (−8)	0.65	4
119	$C^+ + HC_3N \rightarrow C_3^+ + HCN$	1 (−8)	0.65	4
120	$C^+ + HC_3N \rightarrow CNC^+ + C_2H$	4 (−9)	0.65	4
121	$C^+ + C_3N \rightarrow C_3^+ + CN$	1.3 (−7)	0.65	R117
122	$C^+ + HC_5N \rightarrow C_5H^+ + CN$	1.3 (−7)	0.65	R117
123	$C^+ + HC_5N \rightarrow C_5^+ + HCN$	3.6 (−8)	0.65	Estimated
124	$C^+ + HC_5N \rightarrow C_3H^+ + C_3N$	3.6 (−8)	0.65	Estimated
125	$C^+ + C_5N \rightarrow C_5^+ + CN$	1.3 (−7)	0.65	R121
126	$C^+ + HC_7N \rightarrow C_7H^+ + CN$	1.3 (−7)	0.65	R117
127	$C^+ + HC_7N \rightarrow C_5H^+ + C_3N$	2.4 (−8)	0.65	Estimated
128	$C^+ + HC_7N \rightarrow C_3H^+ + C_5N$	2.4 (−8)	0.65	Estimated
129	$C^+ + HC_7N \rightarrow C_7^+ + HCN$	2.4 (−8)	0.65	Estimated
130	$C^+ + C_7N \rightarrow C_7^+ + CN$	8 (−8)	0.65	Estimated
131	$C^+ + C_7N \rightarrow C_5^+ + C_3N$	5.3 (−8)	0.65	Estimated
132	$H_3^+ + C \rightarrow CH + H_2$	2 (−9)	...	3
133	$H_3^+ + CH \rightarrow CH_2^+ + H_2$	1.2 (−9)	...	3
134	$H_3^+ + CH_2 \rightarrow CH_3^+ + H_2$	1.7 (−9)	...	3
135	$H_3^+ + C_2 \rightarrow C_2H^+ + H_2$	1.8 (−9)	...	3
136	$H_3^+ + C_2H \rightarrow C_2H_2^+ + H_2$	1.7 (−9)	...	3
137	$H_3^+ + CO \rightarrow HCO^+ + H_2$	1.7 (−9)	...	4
138	$H_3^+ + N_2 \rightarrow N_2H^+ + H_2$	1.8 (−9)	...	4
139	$H_3^+ + C_2H_2 \rightarrow C_2H_3^+ + H_2$	2.9 (−9)	...	4

APPENDIX B—*Continued*

Number	Reaction	Rate Coefficient[a] A	n	References[b]
140	$H_3^+ + HCN \rightarrow H_2CN^+ + H_2$	3 (−7)	0.65	4
141	$H_3^+ + HNC \rightarrow H_2CN^+ + H_2$	3 (−7)	0.65	4
142	$H_3^+ + HC_3N \rightarrow H_2C_3N^+ + H_2$	4.1 (−7)	0.65	4
143	$H_3^+ + HC_5N \rightarrow H_2C_5N^+ + H_2$	4.1 (−7)	0.65	R142
144	$HCO^+ + C \rightarrow CH^+ + CO$	1.1 (−9)	...	3
145	$HCO^+ + C_2 \rightarrow C_2H^+ + CO$	8.3 (−10)	...	3
146	$HCO^+ + C_2H_2 \rightarrow C_2H_3^+ + CO$	1.4 (−9)	...	4
147	$HCO^+ + C_2H \rightarrow C_2H_2^+ + CO$	4.1 (−8)	0.65	Estimated
148	$HCO^+ + HCN \rightarrow H_2CN^+ + CO$	1.4 (−7)	0.65	4
149	$HCO^+ + HNC \rightarrow H_2CN^+ + CO$	1.4 (−7)	0.65	4
150	$HCO^+ + HC_3N \rightarrow H_2C_3N^+ + CO$	1.5 (−7)	0.65	4
151	$HCO^+ + HC_5N \rightarrow H_2C_5N^+ + CO$	1.5 (−7)	0.65	R150
152	$N_2H^+ + CO \rightarrow HCO^+ + N_2$	8.8 (−10)	...	4
153	$C_2H_2^+ + C_2H_2 \rightarrow C_4H_3^+ + H$	5.9 (−10)	...	11
154	$C_2H_2^+ + C_2H_2 \rightarrow C_4H_2^+ + H_2$	5.2 (−10)	...	11
155	$C_2H_2^+ + C_2H \rightarrow C_4H_2^+ + H$	2 (−8)	0.65	Estimated
156	$C_2H_2^+ + C_2H \rightarrow C_4H^+ + H_2$	2 (−8)	0.65	Estimated
157	$C_2H_2^+ + HCN \rightarrow H_2CN^+ + C_2H$	9.8 (−9)	0.65	4
158	$C_2H_2^+ + HCN \rightarrow H_2C_3N^+ + H$	4.9 (−9)	0.65	4
159	$C_2H_2^+ + CN \rightarrow H_2C_3N^+ + h\nu$	3 (−9)	0.65	Estimated
160	$C_2H_2^+ + HNC \rightarrow H_2CN^+ + C_2H$	9.8 (−9)	0.65	R157
161	$C_2H_2^+ + HNC \rightarrow H_2C_3N^+ + H$	4.9 (−9)	0.65	R158
162	$C_2H_2^+ + HC_3N \rightarrow C_4H_2^+ + HCN$	6.1 (−8)	0.65	4
163	$C_2H_2^+ + HC_3N \rightarrow H_3C_5N^+ + h\nu$	9.2 (−8)	0.65	4
164	$C_2H_2^+ + C_3N \rightarrow C_4H^+ + HCN$	4.1 (−8)	0.65	Estimated
165	$C_2H_2^+ + C_3N \rightarrow C_4H_2^+ + CN$	2 (−8)	0.65	Estimated
166	$C_2H_2^+ + C_3N \rightarrow H_2C_5N^+ + h\nu$	9.2 (−8)	0.65	R163
167	$C_2H_2^+ + HC_5N \rightarrow H_3C_7N^+ + h\nu$	9.2 (−8)	0.65	R163
168	$C_2H_2^+ + HC_5N \rightarrow C_6H_2^+ + HCN$	3 (−8)	0.65	Estimated
169	$C_2H_2^+ + HC_5N \rightarrow C_4H_2^+ + HC_3N$	3 (−8)	0.65	Estimated
170	$C_2H_2^+ + C_5N \rightarrow H_2C_7N^+ + h\nu$	9.2 (−8)	0.65	R163
171	$C_2H_2^+ + C_5N \rightarrow C_6H_2^+ + CN$	1 (−8)	0.65	Estimated
172	$C_2H_2^+ + C_5N \rightarrow C_4H_2^+ + C_3N$	1 (−8)	0.65	Estimated
173	$C_2H_2^+ + C_5N \rightarrow C_6H^+ + HCN$	4.1 (−8)	0.65	R164
174	$C_2H_3^+ + C_2H_2 \rightarrow C_4H_3^+ + H_2$	2.2 (−10)	...	4
175	$C_2H_3^+ + HCN \rightarrow H_2CN^+ + C_2H_2$	6.5 (−8)	0.65	4
176	$C_2H_3^+ + HNC \rightarrow H_2CN^+ + C_2H_2$	6.5 (−8)	0.65	4
177	$C_2H_3^+ + CN \rightarrow H_2CN^+ + C_2H$	4.1 (−8)	0.65	Estimated
178	$C_2H_3^+ + HC_3N \rightarrow H_2C_3N^+ + C_2H_2$	1.6 (−7)	0.65	4
179	$C_2H_3^+ + HC_5N \rightarrow H_2C_5N^+ + C_2H_2$	1.6 (−7)	0.65	R178
180	$C_4H_2^+ + HC_3N \rightarrow H_3C_7N^+ + h\nu$	7 (−8)	0.65	4
181	$C_4H_2^+ + HC_3N \rightarrow C_6H_2^+ + HCN$	4.7 (−8)	0.65	Estimated
182	$C_4H_2^+ + C_3N \rightarrow H_2C_7N^+ + h\nu$	7 (−8)	0.65	R180
183	$C_2H_2^+ + N \rightarrow CNC^+ + H + H$	7.5 (−11)	...	4
184	$C_2H_2^+ + N \rightarrow HCN + CH^+$	2.5 (−11)	...	4
185	$C_2H_2^+ + N \rightarrow HC_2N^+ + H$	1.5 (−10)	...	4
186	$C_2H_4^+ + N \rightarrow H_3C_2N^+ + H$	1.5 (−10)	...	6
187	$C_2H_4^+ + N \rightarrow H_2C_2N^+ + H + H$	7.5 (−11)	...	6
188	$C_2H_2^+ + O \rightarrow HCO^+ + CH$	8.5 (−11)	...	4
189	$lC_3H_3^+ + N \rightarrow H_2C_3N^+ + H$	1.3 (−10)	...	5
190	$cC_3H_3^+ + N \rightarrow H_2C_3N^+ + H$	1.3 (−10)	...	5
191	$C_2H_2^+ + H_2 \rightarrow C_2H_3^+ + H$	5.6 (−11)	2.0	7
192	$C_2H_2^+ + H_2 \rightarrow C_2H_4 + h\nu$	4.7 (−12)	1.33	7
193	$C_2H_4^+ + C_2H_2 \rightarrow cC_3H_3^+ + CH_3$	3.2 (−10)	...	4
194	$C_2H_4^+ + C_2H_2 \rightarrow lC_3H_3^+ + CH_3$	3.2 (−10)	...	4
195	$C_2H_4^+ + HC_3N \rightarrow H_2C_3N^+ + C_2H_3$	4.5 (−8)	0.65	4
	Radical-Molecule Reactions			
196	$C_2H + HCN \rightarrow HC_3N + H$	2.2 (−12)	...	9
197	$C_2H + C_2H_2 \rightarrow C_4H_2 + H$	3.1 (−11)	...	10
198	$C_2H + C_4H_2 \rightarrow C_6H_2 + H$	6.6 (−11)	...	Estimated
199	$CN + C_2H_2 \rightarrow HC_3N + H$	2.3 (−10)	...	6
200	$CN + C_4H_2 \rightarrow HC_5N + H$	2.3 (−10)	...	Estimated
201	$CN + C_6H_2 \rightarrow HC_7N + H$	2.3 (−10)	...	Estimated
202	$C_3N + C_2H_2 \rightarrow HC_5N + H$	3 (−10)	...	Estimated
203	$C_3N + C_2H_2 \rightarrow C_4H_2 + CN$	2.3 (−10)	...	Estimated
204	$C_3N + C_4H_2 \rightarrow HC_7N + H$	3 (−10)	...	Estimated
205	$C_5N + C_2H_2 \rightarrow HC_7N + H$	3 (−10)	...	Estimated
206	$C_5N + C_2H_2 \rightarrow C_6H_2 + CN$	2.3 (−10)	...	Estimated
207	$C + C_2 \rightarrow C_3$	4 (−11)	...	Estimated

APPENDIX B—*Continued*

Number	Reaction	Rate Coefficient[a] A	n	References[b]
208	$C + C_3 \rightarrow C_4$	$4\ (-10)$	...	Estimated
209	$C + C_4 \rightarrow C_5$	$4\ (-10)$	...	Estimated
210	$C + C_2H \rightarrow C_3H$	$4\ (-11)$	...	Estimated
211	$C + C_3H \rightarrow C_4H$	$4\ (-10)$	...	Estimated
212	$C + C_4H \rightarrow C_5H$	$4\ (-10)$	...	Estimated

[a] The rate coefficient are given by $k = AT^{-n}$, where A is in units of $cm^3\ s^{-1}\ K^n$.
[b] Rn refers to the reaction number.
(1) Escalante & Victor 1990.
(2) Mitchell 1990.
(3) Millar et al. 1991.
(4) Anicich & Huntress 1986.
(5) Federer et al. 1986.
(6) Lichtin & Lin 1986.
(7) Glassgold et al. 1992.
(8) Amano 1990.
(9) Yung et al. 1984.
(10) Laufer & Bass 1979.
(11) Anicich 1993.

REFERENCES

Amano, T. 1990, J. Chem. Phys., 92, 6492
Anicich, V. G. 1993, ApJS, 84, 215
Anicich, V. G., & Huntress, W. T. 1986, ApJS, 62, 553
Bieging, J., Chapman, B., & Welch, W. J. 1984, ApJ, 285, 256
Bieging, J., & Rieu, N.-Q. 1988, ApJ, 329, L107
Bieging, J., & Tafalla, M. 1992, ApJ, submitted
Bowen, G. H. 1988, ApJ, 329, 299
Cernicharo, J., Guélin, M., Menten, K. M., & Walmsley, C. M. 1987, A&A, 181, L1
Cherchneff, I., & Barker, J. R. 1992, ApJ, 394, 703
Clary, D. C. 1985, J. Molec. Phys., 53, 3
Colangeli, L., Blanco, A., Fonti, S., & Bussoletti, E. 1992, ApJ, 392, 284
Connors, R. E., Roebber, J. L., & Weiss, K. 1974, J. Chem. Phys., 60, 5011
Crabtree, D. R., McLaren, R. A., & Christian, C. A. 1987, in Late Stages of Stellar Evolution, ed. S. Kwok & S. P. Pottasch (Dordrecht: Reidel), 145
Danchi, W. C., Bester, M., Degiacomi, C. G., McCullough, P. R., & Townes, C. H. 1990, ApJ, 359, L59
Désert, F. X., Bazell, D., & Boulanger, F. 1988, ApJ, 334, 815
Draine, B. T. 1978, ApJS, 36, 595
Escalante, V., & Victor, G. A. 1990, ApJS, 73, 513
Federer, W., Villinger, H., Lindinger, W., & Ferguson, E. E. 1986, Chem. Phys. Lett., 123, 12
Glassgold, A. E., Lucas, R., & Omont, A. 1986, A&A, 157, 35 (GLO)
Glassgold, A. E., & Mamon, G. A. 1992, Chemistry and Spectroscopy of Interstellar Molecules, ed. N. Kaifu (Tokyo: Univ. Tokyo Press), 261
Glassgold, A. E., Mamon, G. A., Omont, A., & Lucas, R. 1987, ApJ, 180, 183 (GMOL)
Glassgold, A. E., Mamon, G. A., & Huggins, P. J. 1991, ApJ, 373, 254
Glassgold, A. E., Omont, A., & Guélin, M. 1992, ApJ, 396, 115
Gondhalekar, P. M. 1990, The Galactic and Extragalactic Background Radiation, ed. S. Bowyer & C. Leinert (Dordrecht: Reidel), 49
Guélin, M., & Cernicharo, J. 1991, A&A, 244, L21
Herbst, E., & Leung, C. M. 1986, ApJ, 310, 378
Howe, D. A., & Millar, T. J. 1990, MNRAS, 244, 444
Huggins, P. J., & Glassgold, A. E. 1982, ApJ, 252, 201
Huggins, P. J., Glassgold, A. E., & Morris, M. 1984, ApJ, 279, 284
Huggins, P. J., Olofson, H., & Johansson, L. E. B. 1988, ApJ, 332, 1009
Irvine, W. M., et al. 1988, ApJ, 334, L107
Jura, M. 1974, ApJ, 191, 375
Jura, M., & Kroto, H. 1990, ApJ, 351, 222
Keady, J. J., & Ridgway, S. T. 1993, ApJ, 406, 199
Lafont, S., Lucas, R., & Omont, A. 1982, A&A, 106, 201
Laufer, A. M., & Bass, A. M. 1979, J. Phys. Chem., 83, 310
Lavendy, H., Robbe, J. M., & Gandara, G. 1987, J. Phys. B, 20, 3067
Le Bertre, T. 1987, A&A, 176, 107
Lee, L. C. 1980, J. Chem. Phys., 72, 6414
———. 1984, ApJ, 282, 172
Lichtin, D. A., & Lin, M. C. 1986, Chem. Phys., 104, 325
Lucas, R. 1992, Astrochemistry of Cosmic Phenomena, ed. P. D. Singh (Dordrecht: Kluwer), 389
Lucas, R., & Guélin, M. 1988, Submillimeter and Millimeter Astronomy, ed. W. B. Burton & R. D. Wolstencroft (Dordrecht: Reidel), 97
Magnani, L., Blitz, L., & Mundy, L. 1985, ApJ, 295, 402
Mamon, G. A., Glassgold, A. E., & Huggins, P. J. 1988, ApJ, 327, 797
Martin, P. G., & Rodgers, C. 1987, ApJ, 322, 373
May, J., Murphy, D. C., & Thaddeus, P. 1988, A&AS, 73, 51
Millar, T. J., Rawlings, J. M. C., Bennett, A., Brown, P. D., & Charnley, S. B. 1991, A&AS, 87, 585
Mitchell, J. B. A. 1990, Phys. Rep., 186, 217
Morris, M., & Jura, M. 1983, ApJ, 264, 546
Nakano, T., & Tademaru, E. 1972, ApJ, 173, 87
Nakayama, T., & Watanabe, K. 1964, J. Chem. Phys., 40, 558
Nejad, L. A. M., & Millar, T. J. 1987, A&A, 183, 279
Pauzat, F., Ellinger, Y., & McLean, A. D. 1991, ApJ, 369, L13
Pouilly, B., Robbe, J. M., Schamps, J. S., & Roueff, E. 1983, J. Phys. B, 16, 437
Roberge, W. G., Jones, D., Lepp, S., & Dalgarno, A. 1991, ApJS, 77, 287
Rouleau, F., & Martin, P. G. 1991, ApJ, 377, 526
Rowe, B. R., Canosa, A., & Sims, I. 1993, J. Chem. Soc. Faraday Trans., in press
Smith, P. L., Yoshino, K., & Parkinson, W. H. 1991, J. Geophys. Res., 96, 17529
Sopka, R. J., Hildebrand, R., Jaffe, D. T., Gatley, I., Roellig, T., Werner, M., Jura, M., & Zuckerman, B. 1985, ApJ, 294, 242
Spitzer, L., Jr., & Tomasko, M. 1968, ApJ, 152, 971
Stoecklin, T., Dateo, C. E., & Clay, D. C. 1991, J. Chem. Soc. Faraday Trans., 87, 1667
Suto, M., & Lee, L. C. 1985, J. Geophys. Res., 90, 13037
Tielens, A. G. G. M. 1992, Planetary Nebulae, ed. R. Weinberger & A. Acker (Dordrecht: Reidel), in press
Truong-Bach, Rieu, N.-Q., Omont, A., Oloffson, H., & Johansson, L. E. B. 1987, A&A, 176, 285
van Dishoeck, E. F. 1988, Rate Coefficients in Astrochemistry, ed. T. J. Millar & D. A. Williams (Dordrecht: Kluwer), 49
van Dishoeck, E. F., & Black, J. H. 1986, ApJS, 62, 109
Viala, Y. P. 1986, A&AS, 64, 391
Wiedemann, G. R., et al. 1991, ApJ, 382, 321
Wu, C. Y., Chien, T. S., Liu, G. S., & Judge, D. L. 1989, J. Chem. Phys., 91, 272
Wu, C. Y. R., & Judge, D. L. 1985, J. Chem. Phys., 82, 4495
Yung, Y. L., Allen, M., & Pinto, J. P. 1984, ApJS, 55, 465
Zuckerman, B., Dick, H. M., & Claussen, M. J. 1986, ApJ, 304, 401